Geochemical Perspectives Letters

The vanadium isotope composition of Mars: implications for planetary differentiation in the early solar system

S.G. Nielsen, D.V. Bekaert, T. Magna, K. Mezger, M. Auro

Supplementary Information

The Supplementary Information includes:

1. Methods

Powdered samples (30–90 mg) were dissolved using double-distilled concentrated HF, HNO_3, and HCl. Vanadium was separated from the sample matrix using a four-step cation/anion exchange chromatography procedure described in detail elsewhere (Nielsen *et al.*, 2011, 2019). Briefly, the method comprises one cation exchange resin column in 1M HNO_3, followed by three anion exchange resin columns where V is bound to the resin by complexation with H_2O_2 (Nielsen *et al.*, 2011). Throughout the study chemical yields were >80% and were monitored for by comparing the mass of V recovered from the ion exchange chemistry with the amount of V processed, which was based on either V concentrations measured in each sample or collected from literature data. Blanks were monitored with each batch of samples and were always <2 ng, which is insignificant compared with the >1000 ng V processed for each sample.

Vanadium isotope ratios were measured using a Neptune multiple-collector inductively-coupled-plasma mass spectrometer (MC-ICPMS), housed at the Plasma Mass Spectrometry Facility of the Woods Hole Oceanographic Institution (WHOI). Isotope compositions were determined using standard–sample bracketing with the Alfa Aesar reference solution that is defined as $\delta^{51}V = 0‰$ (Nielsen *et al.*, 2011). Each unknown sample was interspersed with a pure V reference solution from BDH Chemicals that has now been measured in eight separate studies with the identical

$\delta^{51}V = -1.18 \pm 0.02$‰ (2SE) (Nielsen *et al.*, 2011; Wu *et al.*, 2016; Prytulak *et al.*, 2017; Schuth *et al.*, 2017; Sossi *et al.*, 2017; Nielsen *et al.*, 2019; Wu *et al.*, 2019). The mass spectrometer was operated in medium resolution mode. To quantify and correct for isobaric interferences of ^{50}Ti and ^{50}Cr on ^{50}V the masses ^{48}Ti, ^{49}Ti, ^{52}Cr and ^{53}Cr were monitored and a mass bias correction routine using ^{49}Ti/^{50}Ti and ^{53}Cr/^{50}Cr ratios was applied (Nielsen *et al.*, 2016; Wu *et al.*, 2016). Mass ^{51}V was collected using a Faraday cup equipped with a 10^{10} Ω resistor, whereas Faraday cups with conventional 10^{11} Ω resistors were used to collect all other masses. Samples and standards were measured at a concentration of 800 ng/ml V, which produced an ion beam of ~2 nA on ^{51}V and ~0.005 nA on ^{50}V. Precision and accuracy of the V isotope measurements was assessed by measuring the BDH standard throughout the study (covering the period from February 2015 to September 2018) and by processing USGS reference materials AGV-2 and BCR-2 with every batch of unknown samples. These reference materials have previously been analyzed by different laboratories (Nielsen *et al.*, 2019). The resulting mean $\delta^{51}V$ values for AGV-2 and BCR-2 for the entire analytical period were -0.73 ± 0.15‰ (2SD; n = 47) and -0.83 ± 0.20‰ (2SD; n = 65), respectively, which is in excellent agreement with previous studies (Prytulak *et al.*, 2011, 2013; Wu *et al.*, 2016, 2018; Nielsen *et al.*, 2019). These external errors are similar to those obtained for the martian meteorites that exhibit 2SD from 0.06 to 0.24‰ (Table 1).

Elemental concentrations were determined for a subset of the samples using a ThermoFinnigan iCap quadrupole ICP-MS, housed at the WHOI Plasma Mass Spectrometry Facility. Concentrations were calculated via reference to ion beam intensities obtained from a five-point calibration curve constructed from serial dilutions of a gravimetrically-prepared multi-element standard; drift was monitored and corrected via normalization to indium intensities. Accuracy and precision were better than ± 7% (2SE) based on the correspondence of concentrations in USGS reference materials AGV-2, BCR-2, and BHVO-2 determined during the same analytical sessions as the martian meteorites.

2. Uniformity of the V isotope composition of martian rocks

Previous studies have demonstrated that GCR spallation produces ^{50}V, which in some cases can be critical to correct for (Hopkins *et al.*, 2019). All the martian meteorites investigated here have relatively young cosmic ray exposure ages (<15 Ma for nakhlites and ALH84001, <5 Ma for shergottites (e.g. Nyquist *et al.*, 2001)) and, compared with most other meteorites from different parent bodies, relatively high V contents, which results in corrections for GCR spallation of <0.03‰ (Table 1). These corrections are based on the correlations between cosmic ray exposure (CRE) ages and V isotope compositions of lunar rocks (Hopkins *et al.*, 2019). Application of the lunar rock calibration curve to other types of meteorites can be associated with significant systematic errors. However, given the very small total GCR corrections required for martian meteorites, it can be concluded that the corrections, as implemented here, are unlikely to induce any additional error on the V isotope compositions, because the average spallation correction for all martian meteorites is <0.01‰.

After correction for spallation effects, we investigated possible V isotope variations within the V isotope dataset for martian meteorites. These were performed by carrying out Monte Carlo simulations using the raw data and their associated uncertainties to artificially generate 1 million datasets for basaltic shergottites, olivine-phyric shergottites, lherzolitic shergottites, nakhlites and orthopyroxenite, and hence compute 1 million $\delta^{51}V$ mean values for each type of rocks. At each iteration step, the mean composition of olivine-phyric shergottites is compared to that of the other rocks ($\Delta^{51}V_{Ops\text{-}Smpl} = \delta^{51}V_{Ops} - \delta^{51}V_{Smpl}$, where "Ops" and "Smpl" correspond to olivine-phyric shergottites and other rock samples, respectively). Olivine-phyric shergottites were chosen here for reference, as they are the type of martian meteorites for which we have analyzed the most samples (and so for which we have the best statistics). Computed $\Delta^{51}V_{Ops\text{-}Smpl}$ are shown in Figure S-1, demonstrating that the V isotope composition of basaltic shergottites, lherzolitic shergottites, nakhlites and orthopyroxenite are statistically indistinguishable from that of olivine-phyric shergottites. The error-weighted average V isotope composition measured for the 24 martian meteorites is hence used to derive the best estimate for the V isotope composition of Bulk Silicate Mars (BSM), which yields $\delta^{51}V = -1.026 \pm 0.029$‰ (2SE, MSWD=0.99).

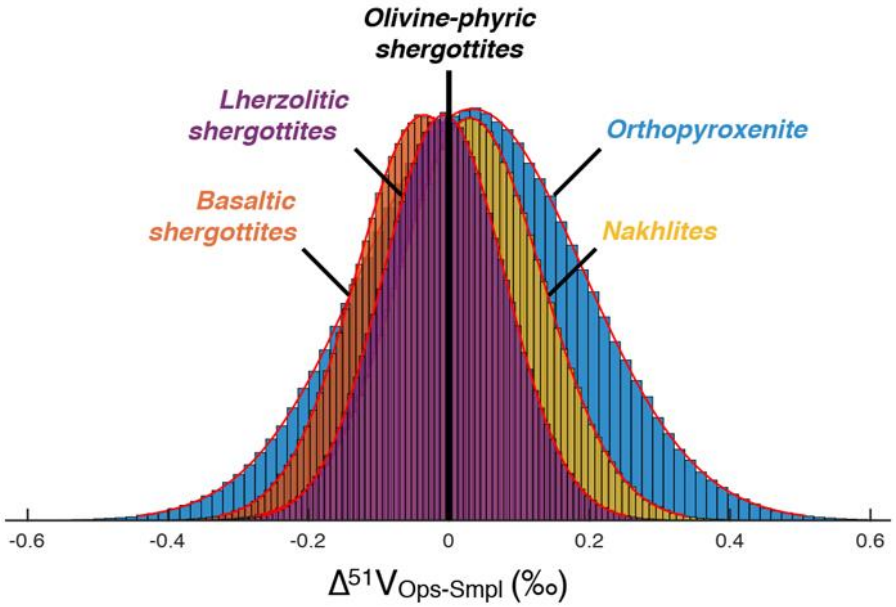

Figure S-1 Mean V isotope compositions of basaltic shergottites, lherzolitic shergottites, nakhlites and orthopyroxenite compared to that of olivine-phyric shergottites ($\Delta^{51}V_{Ops\text{-}Smpl}$) as generated by our Monte Carlo simulations (1 million runs).

Calculation of an average value for BSM and application of the 2SE uncertainty to this number requires that all individual data (i) originate from a unique population and (ii) are normally distributed around the mean (real) value of the population. To ascertain whether the martian data have come from a normally distributed population, we present a quantile-quantile (Q-Q) plot of the martian V isotope data (Fig. S-2). This plot corresponds to a graphical method for comparing two probability distributions - here the quantiles of the sample datasets versus theoretical quantile values generated from normal distributions - by plotting their quantiles against each other. The fact that the data broadly plot along a straight line in this Q-Q plot indicates that the martian V isotope dataset is consistent with a Gaussian distribution. However, these graphical considerations do not allow quantitatively validating/refuting the hypothesis of the dataset being normally distributed, and further statistical tests are required.

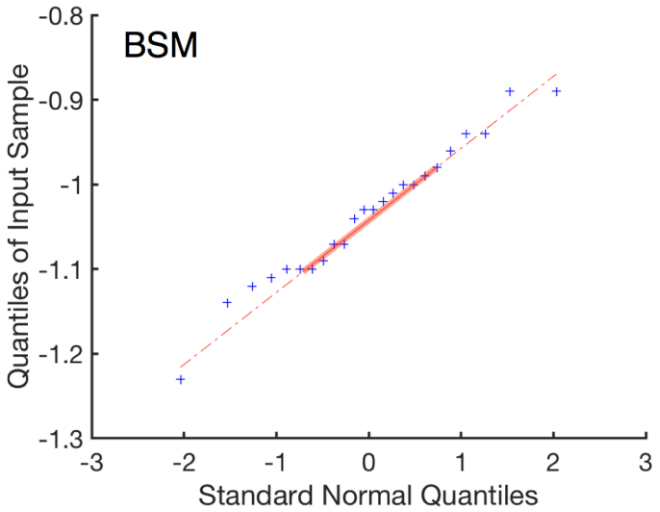

Figure S-2 Results of quantile-quantile calculations with the quantiles of the sample dataset plotted against theoretical quantile values generated from normal distributions. The linear relationship implies that the martian V isotope data are consistent with a normally distributed data population.

To further investigate whether the martian data have come from a normally distributed population, a series of Anderson-Darling normality tests was performed using the same Monte Carlo approach as for the Student's t-test. The Monte Carlo approach was chosen because Anderson-Darling and Student's t-tests are only based on the distribution of the data and do not take into account uncertainties associated with each individual datapoint. In order to overcome this caveat and compensate for the small size of the datasets, we used Monte Carlo simulations to artificially generate 1 million datasets for the BSM from the raw data and associated uncertainties. For each dataset, we postulate the null hypothesis that the generated dataset is from a population with a normal distribution. The Anderson-Darling test then returns a decision for the null hypothesis at the 5% significance level. After 1 million iterations, it is found that 90.5% of the tests did not reject the null hypothesis of normality, which further supports the conclusion that our data set is part of a normally distributed population.

3. V isotope composition of bulk silicate Earth

It has previously been argued that mantle melting on Earth might induce V isotope fractionation towards both lighter and heavier compositions (Prytulak *et al.*, 2013; Qi *et al.*, 2019). Therefore, it was suggested that fertile peridotites were the most appropriate samples to use for estimating the V isotope composition of the bulk silicate Earth (BSE) (Prytulak *et al.*, 2013; Qi *et al.*, 2019). However, this conclusion is at odds with the fact that both fertile and strongly melt depleted peridotites are indistinguishable in terms of V isotopes (Qi *et al.*, 2019), which would imply no detectable V isotope fractionation during melting. Likewise, extensive fractional crystallization does impart significant V isotope fractionation (Prytulak *et al.*, 2017), in particular if magnetite is removed from the melt during crystallization (Prytulak *et al.*, 2017; Sossi *et al.*, 2018). However, there is no evidence to suggest that V isotopes are fractionated during removal of early crystallizing phases such as olivine, orthopyroxene and clinopyroxene.

Figure S-3 shows the Probability Density Functions (PDF) of $\delta^{51}V$ for all available literature data on terrestrial rocks (Table S-1), which are then compared to each other in Figure S-4. When compiling all data from unaltered peridotites ($\delta^{51}V = -0.829 \pm 0.050$; n = 22, 2SE), unaltered mid ocean ridge basalts (MORBs) ($\delta^{51}V = -0.862 \pm 0.026$; n = 29, 2SE), komatiites ($\delta^{51}V = -0.872 \pm 0.030$; n = 14, 2SE), and ocean island basalts (OIBs) ($\delta^{51}V = -0.870 \pm 0.044$; n = 11; 2SE), it becomes clear that peridotites are indistinguishable from mantle melts and, therefore, all of these samples should be included in the best estimate for the BSE composition. This finding is notably underscored by Student's t-tests giving p-values of 0.25, 0.23, and 0.15 when peridotites are compared with MORBs, OIBs, and komatiites, respectively (Table S-1).

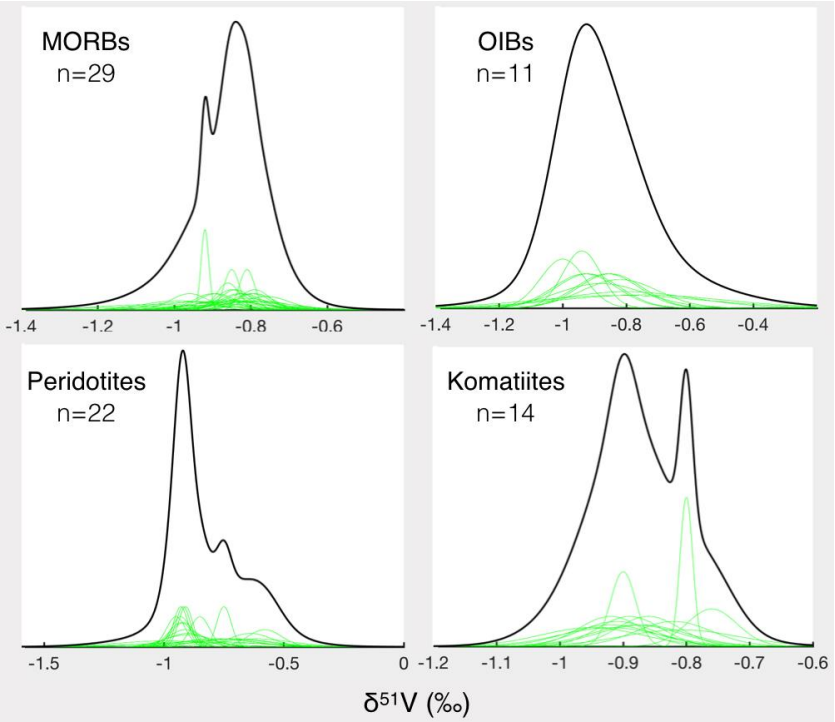

Figure S-3 PDF of $\delta^{51}V$ for all available literature data on terrestrial rocks (Table S-1). The numbers of samples (n) are reported for each type of terrestrial rock considered here.

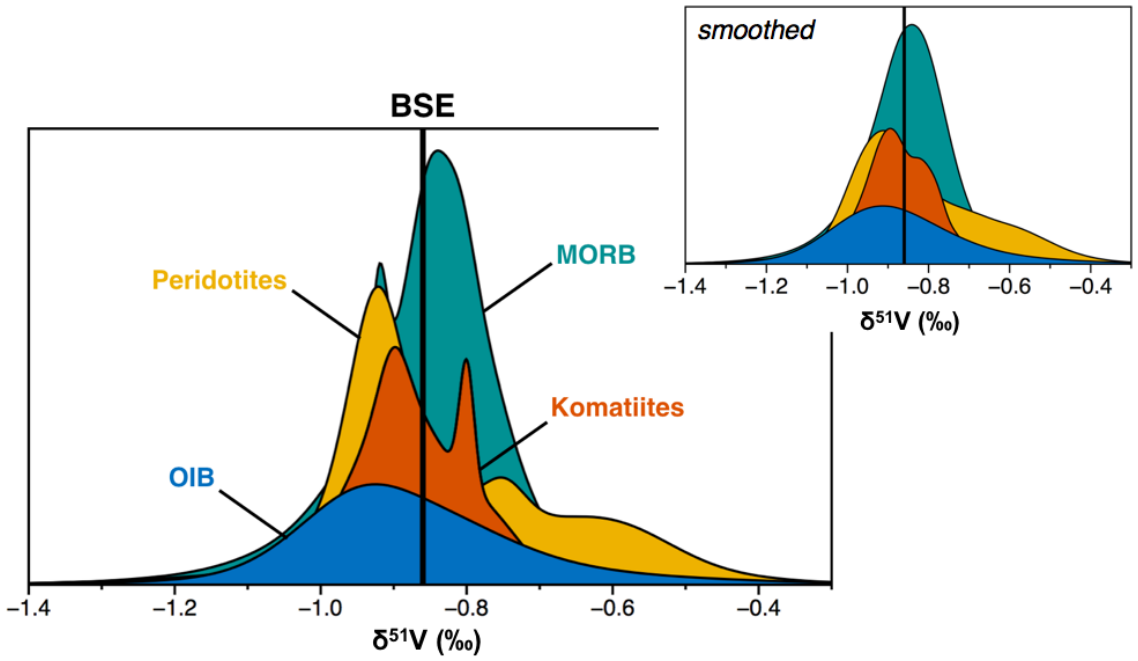

Figure S-4 Summary plot of the PDF of $\delta^{51}V$ for the four types of terrestrial rock considered here. Our computed mean composition of the BSE is reported as a vertical black line. The top right subpanel shows a smoothed version of these PDF.

In order to compensate for the limited size of our datasets and provide a meaningful statistical assessment of potential V isotope variations across terrestrial rocks, we carried out Monte Carlo simulations using the raw data and

their associated uncertainties to artificially generate 1 million datasets for peridotites, MORBs, komatiites and OIBs, and hence compute 1 million $\delta^{51}V$ mean values for each rock type. At each iteration step, the mean compositions of peridotites, komatiites and OIBs are compared to that of MORBs ($\Delta^{51}V_{MORB\text{-}Res.} = \delta^{51}V_{MORB} - \delta^{51}V_{Res.}$, where "Res." corresponds to peridotites, komatiites or OIBs). Computed $\Delta^{51}V_{MORB\text{-}res.}$ are shown in Figure S5, altogether with the 1SD envelope of the MORB mean value obtained for the 1 million runs. Here again, it appears that peridotites, komatiites and OIBs are statistically indistinguishable from MORBs (Figure S-5).

We therefore conclude that, even though it is possible that V isotopes are fractionated to some extent during mantle melting, current literature data as a whole do not demonstrate this process to operate. Therefore, it appears reasonable to compile all currently available V isotope data for relatively primitive mantle melts and peridotites that have not been significantly hydrothermally altered to obtain a more robust estimate for BSE, covering wide ranges of geographic dispersion, degrees of melting, as well as mantle source regions. All together we include 76 samples in our compilation (Prytulak *et al.*, 2011, 2013; Wu *et al.*, 2016, 2018; Qi *et al.*, 2019) (Table S1) and obtain an average value for BSE of $\delta^{51}V_{BSE} = -0.856 \pm 0.020$‰ (2SE). It is worth noting that this value is within error of previous estimates for BSE (Prytulak *et al.*, 2013; Qi *et al.*, 2019), but given the larger and more robust data set used here, it is much more precise.

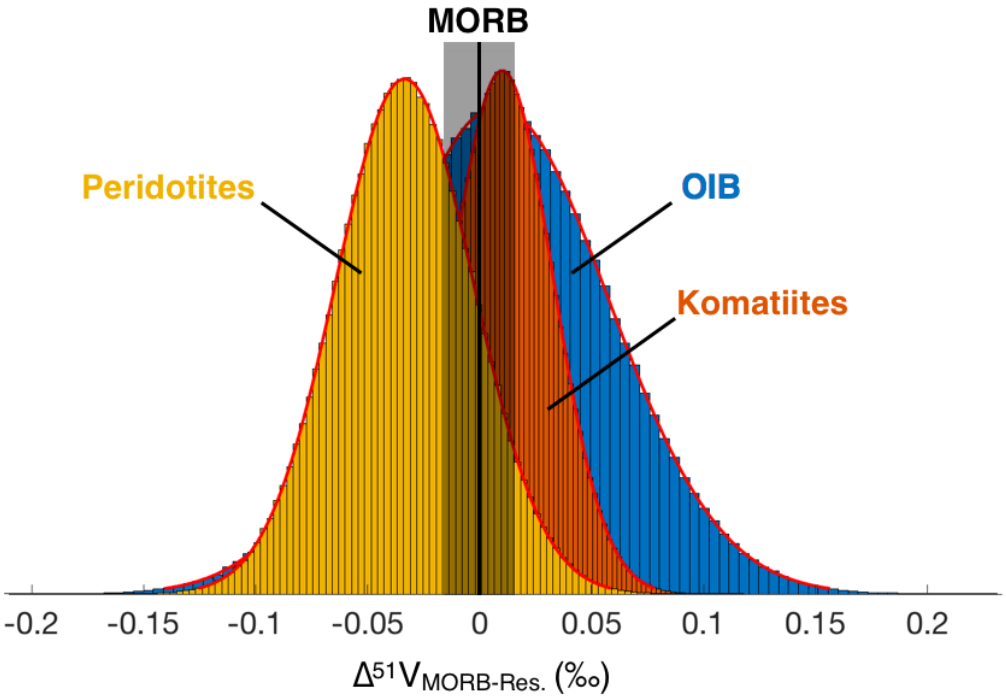

Figure S-5 Mean V isotope compositions of peridotites, komatiites and OIBs compared to that of MORBs ($\Delta^{51}V_{MORB\text{-}Res.}$) as generated by our Monte Carlo simulations (1 million runs). The mean and 1SD envelope of the MORB $\delta^{51}V_{MORB}$ as derived from these Monte Carlo simulations are reported as a vertical line and grey area, respectively.

Although the present estimate for BSE consists of a relatively large data set, it is still possible that some V isotopic heterogeneity exists in the Earth's mantle that has not yet been discovered. For example, early magma ocean crystallization on Earth could potentially have induced significant V isotope fractionation. Although mantle convection over Earth history is likely to have erased most of such potential variation, remnant isotopic heterogeneities inherited from early Earth processes clearly remain for some elements other than vanadium (Rizo *et al.*, 2016). Most likely, such variation would be found in the deep mantle that is much more sporadically sampled than the uppermost portion of the mantle, from which MORBs and most peridotites derive. However, the present estimate of the V isotope composition of BSE does include OIBs and komatiites that both sample deeper portions of the mantle. These data do not support the

existence of significant V isotopic heterogeneity in the deep mantle, therefore strengthening the case for our $\delta^{51}V_{BSE}$ estimate to be representative of the BSE composition.

4. V isotope composition of chondrites

Although chondrites on average exhibit relatively short exposure ages, it has been shown that GCR corrections can be significant for some samples (Hopkins *et al.*, 2019). Here we correct for production of ^{50}V in chondrites and thereby investigate the amount of V isotope variation in chondrites. We calculate the irradiation free V isotope compositions for 14 chondrites (Table S-2) and find that after correction for GCR effects there is no detectable variation within error among all the investigated samples, which is in agreement with conclusions from a previous study(Hopkins *et al.*, 2019). Given that the GCR corrected V isotope compositions of all carbonaceous, ordinary, enstatite and rumuruti chondrites are within error of each other, we calculate the error-weighted average chondritic V isotope composition to be $\delta^{51}V_{ch.}$ = -1.089 ± 0.029 ‰ (n = 14, 2SE). This value is identical to an unweighted average of all the data, which yields a value of -1.094 ± 0.030 ‰ (n = 14, 2SE).

It should be noted that there are significant uncertainties associated with correcting for GCR effects in general. In particular, the magnitude of GCR effects not only depends on the CRE age that is calculated based on noble gas isotope compositions of Ne, Ar or Kr, but also depends on the concentrations of potential target nuclei. Importantly, effects from neutron capture are not significant for vanadium (Hopkins *et al.*, 2019), which renders the comparison between CRE ages based on noble gases and V isotope anomalies more robust. However, in addition to Fe there are GCR spallation reactions that involve target nuclei of Ti and Cr that can lead to production of ^{50}V (Hopkins *et al.*, 2019). Because lunar rocks and chondrites can have very different abundances of Cr and, in particular, Ti, it is possible that application of the lunar GCR correction equation to chondrites is associated with a systematic error that would render the corrected chondrite average value incorrect. However, there are several reasons why such an effect, if present, does not significantly affect the average chondrite values calculated here. First, the corrections on chondrites are small (<0.3‰) and, therefore, the systematic error would have to be very large to impact corrected V isotope compositions. Second, theoretical calculations have shown that isotopes of Ti are the most likely alternative targets that can produce ^{50}V whereas the predicted effects from isotopes of Cr are likely negligible (Hopkins *et al.*, 2019). Chondrites uniformly have Ti concentrations around one order of magnitude or more lower than lunar rocks. Hence, if irradiation effects on Ti were significant then we would expect smaller associated corrections on chondrites than when using the GCR correction equation that only includes Fe as a target. For example, if we use (Fe+Ti)/V as a scaling factor in Fig. 1 instead of just Fe/V, then we obtain an error-weighted average GCR-corrected chondrite value of $\delta^{51}V_{ch.}$ = -1.137 ± 0.058‰ (2SE).

5. V isotope difference between the BSE, BSM and Chondrites

We carried out Monte Carlo simulations using the raw data for the BSM, BSE, and Chondrite data sets and their associated individual uncertainties to artificially generate 1 million datasets, and hence compute 1 million $\delta^{51}V$ mean values for the BSM, BSE, and Chondrites. The results of these simulations are shown in Figure S-6. These demonstrate that BSE is substantially heavier than both BSM and chondrites.

At each iteration step, the difference between the mean $\delta^{51}V$ of the BSM and Chondrites was computed as $\Delta^{51}V_{BSM\text{-}Chondrites} = \delta^{51}V_{BSM} - \delta^{51}V_{Chondrites}$. The distribution of $\Delta^{51}V_{BSM\text{-}Chondrites}$ values is shown in Figure S7, demonstrating that the probability for the BSM to have a higher mean $\delta^{51}V$ than Chondrites (i.e., $\Delta^{51}V_{BSM\text{-}chondrites} > 0$) is high (87.13%). These simulations demonstrate that a shift of 0.058 ± 0.051‰ (1SD) exists between the V isotope compositions of the BSM and Chondrites (Figure S-7). This is further substantiated by two-sample *t*-tests that return a test decision for the null hypothesis that the 1 million mean $\delta^{51}V$ values of the BSM and Chondrites come from independent random samples from normal distributions with equal means and equal but unknown variances. The alternative hypothesis is that these two data sets come from populations with unequal means. We carried out 100 two-sample *t*-tests for each time 1 million $\delta^{51}V$ values of the BSM and Chondrites and found that the null hypothesis was systematically rejected at the 5% significance level. This clearly demonstrates that the V isotope compositions of the BSM and Chondrites represent two populations with unequal means.

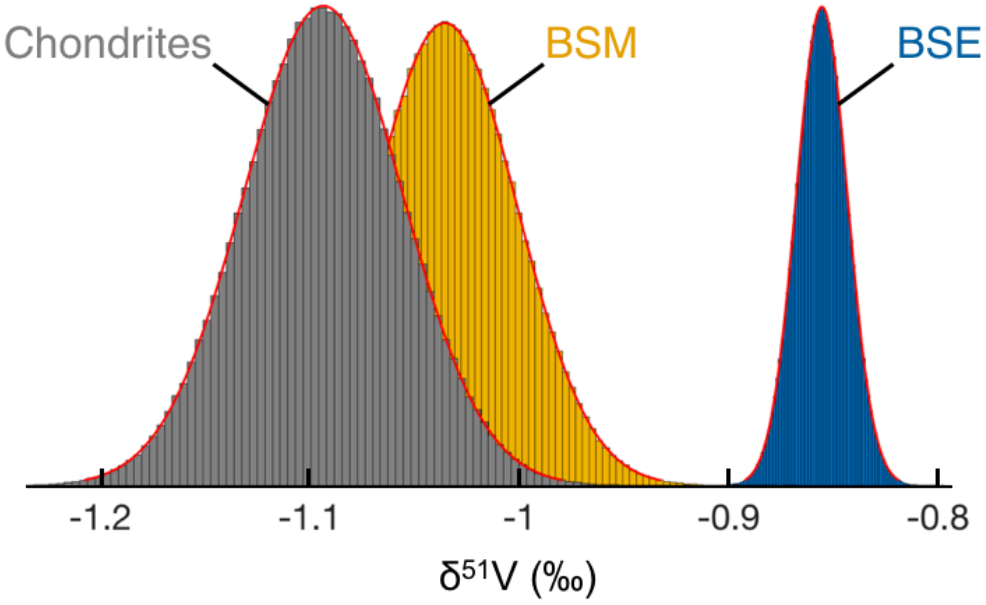

Figure S-6 Average V isotope compositions of chondrites, BSM, and BSE with their probability distributions based on 1 million Monte Carlo simulations of the available data (n= 14, 24 and 76 for Chondrites, BSM and BSE, respectively) and their associated 2SD error bars. Hence, the generated data populations take the full individual errors into account when generating the populations' averages. These show that BSE and BSM are both statistically more enriched in ^{51}V relative to chondrites.

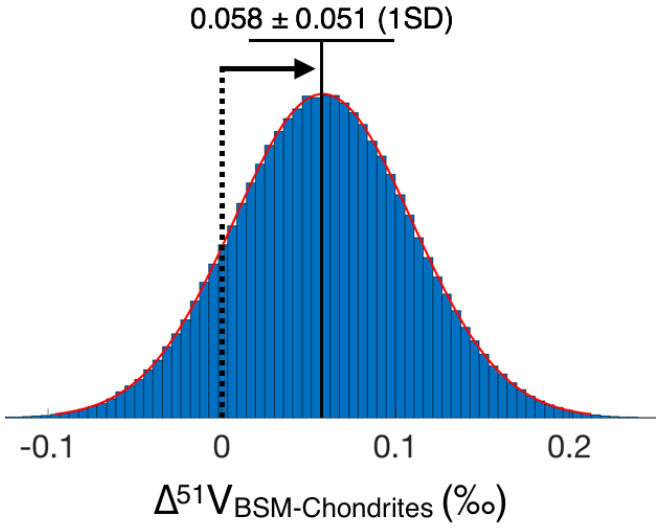

Figure S-7 Frequency distribution of the V isotope difference between the BSM and Chondrites ($\Delta^{51}V_{BSM\text{-}Chondrites}$) as generated by Monte Carlo simulations where the raw data and their associated uncertainties are used to artificially generate 1 million mean $\delta^{51}V_{BSM}$ and $\delta^{51}V_{Chondrites}$ values.

6. Assessment of vanadium depletion in bulk silicate Mars

Little previous quantitative work has been done to assess the extent of V depletion in BSM. Recently, Yoshizaki and McDonough (2020) used refractory lithophile element (RLE) ratio plots for martian meteorites to investigate whether these elements are present in chondritic proportions in BSM. They concluded that, similar to RLE, V was depleted in BSM relative to chondrites by not more ~10%. However, no details of this estimate were given. Here we follow the same approach as Yoshizaki and McDonough (2020) and construct two separate plots using V/Sc vs Y/Ca and V/Lu vs Yb/Ca. All elemental ratios are normalized to chondrites – considered as the bulk Mars composition – to tentatively assess the degree of V depletion in BSM (Fig. S8). In agreement with the analogous plots shown by Yoshizaki and McDonough (2020), the martian meteorite data exhibit significant scatter that may be due to a combination of factors such as analytical uncertainties, sample heterogeneity, fractional crystallization, and melting. However, it is notable that almost all martian meteorites exhibit lower V/Sc and V/Lu ratios than chondrites. Furthermore, if it is assumed that the two RLE ratios (i.e. Y/Ca and Yb/Ca) are present in BSM at the chondritic ratio (Yoshizaki and McDonough, 2020), then the intersection of the correlated data scatter with the chondritic Y/Ca and Yb/Ca ratios can be used to define a potential range of V/Sc (0.40–0.73) and V/Lu (0.37–0.77) in BSM relative to chondrites (Fig. S8). This approach hence enables a first-order assessment of V depletion in BSM, which results in a range of 27% to 60% based on the range of overlap between the V depletion estimates from V/Sc and V/Lu. It should be emphasized that this approach has its own limitations and it is not an attempt to provide a statistically robust best estimate for the V depletion in Mars, given the large scatter of the data. However, due to the almost uniform sub-chondritic V/Sc and V/Lu ratios in martian meteorites (Fig. S-8), it is highly likely that BSM is characterized by a significant V deficit relative to chondrite, which is best explained by V sequestration into the martian core.

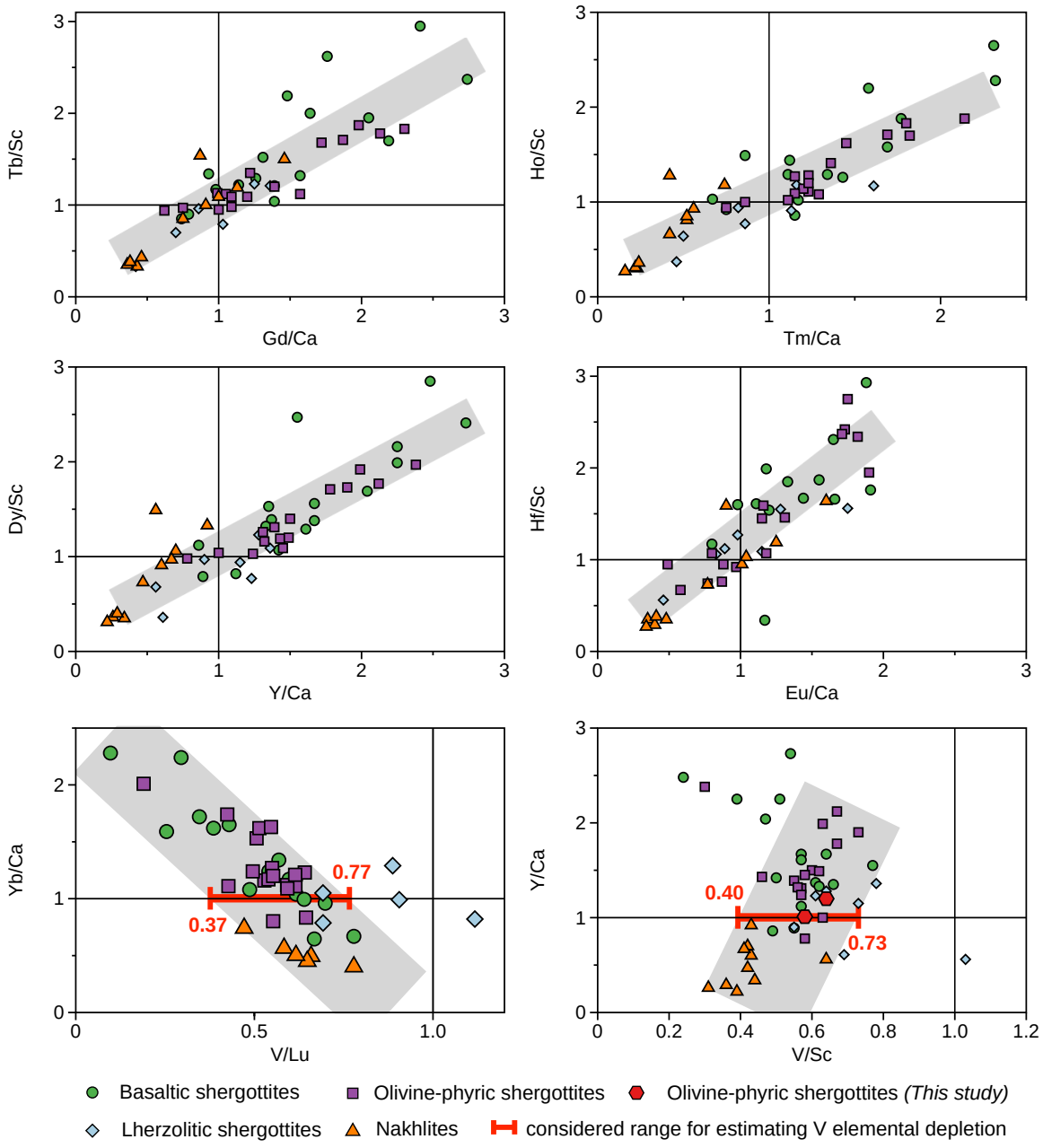

Figure S-8 Ratio/ratio plots of refractory lithophile elements in martian meteorites, normalized to CI chondrite abundances (Yoshizaki and McDonough, 2020). Chemical trend lines reflecting melt-residue differentiation in the martian silicate mantle, represented by the grey areas, appear to cross CI chondrite compositions for all elemental ratios except those involving V, hence pointing to a significant V depletion in martian meteorites relative to chondrites. Unless specified, data are from the compilation by Yoshizaki and McDonough, 2020.

Table S-1 V isotope data included in BSE estimate.

Sample name	Rock type	$\delta^{51}V$	error (2sd)[#]	references
	MORB			
HLY102D73	Basalt	-0.83	0.05	7
HLY102 D8	Basalt	-0.82	0.05	7
HLY102D26	Basalt	-0.81	0.07	7
HLY102D27	Basalt	-0.81	0.02	7
Vema33 D1-2	Basalt	-0.80	0.05	7
DR07-1	Basalt	-0.79	0.10	7
DR05-1	Basalt	-0.79	0.05	7
AII127D46-7	Basalt	-0.79	0.04	7
HLY102D38	Basalt	-0.76	0.06	7
2368-4	Basalt	-0.90	0.05	7
2737-8	Basalt	-0.89	0.05	7
2359-4	Basalt	-0.86	0.03	7
2392-9	Basalt	-0.86	0.10	7
2746-9	Basalt	-0.81	0.07	7
2746-14	Basalt	-0.79	0.09	7
264-04	Basalt	-0.96	0.10	7
265-05	Basalt	-0.93	0.10	7
265-113	Basalt	-0.86	0.08	7
J2-265-88	Basalt	-0.86	0.09	7
J265-82	Basalt	-0.85	0.02	7
266-33	Basalt	-0.84	0.04	7
266-01	Basalt	-0.82	0.09	7
265-49	Basalic andesite	-0.85	0.04	7
TR 16D 1g	Basalt	-1.04	0.15	3
MD57	Basalt	-0.99	0.09	3
POS210/1	Basalt	-0.97	0.22	3
TR30D 2g	Basalt	-0.96	0.05	3
TR 6D 2g	Basalt	-0.92	0.01	3
TR 15D 1g	Basalt	-0.84	0.15	3
	MORB Average (2SE)	-0.862	(0.026)	
	OIB			
BHVO-2	Hawaii	-0.86	0.10	9
BIR-1a	Iceland	-0.92	0.10	4,8,9
4567 45	Tholeiitic basalt Iceland	-1.00	0.07	3
408673	Tholeiitic basalt Iceland	-0.94	0.06	3
4567 49	Tholeiitic basalt Iceland	-0.93	0.10	3
4567 32	Tholeiitic basalt Iceland	-0.88	0.14	3
4567 40	Tholeiitic basalt Iceland	-0.85	0.10	3
4567 43	Tholeiitic basalt Iceland	-0.82	0.27	3
4567 14	Tholeiitic basalt Iceland	-0.82	0.12	3
4567 36	Tholeiitic basalt Iceland	-0.80	0.21	3
4567 22	Tholeiitic basalt Iceland	-0.75	0.26	3
	OIB Average (2SE)	-0.870	(0.044)	

	Komatiites/picrites			
89104	picrite	-0.8	0.01	4
89105/1	picrite	-0.76	0.04	4
9704	Ol-Px cumulate	-0.81	0.09	4
9705	Ol-Px cumulate	-0.82	0.06	4
91117	komatiite	-0.92	0.08	4
91106	komatiite	-0.86	0.05	4
TN2	komatiite	-0.95	0.08	4
TN10	komatiite	-0.9	0.02	4
ALX02	komatiite	-0.88	0.07	4
PH18	komatiite	-0.87	0.07	4
12-2	komatiite	-0.92	0.05	4
501-2	komatiite	-0.89	0.05	4
BV05	komatiite	-0.91	0.06	4
BV15	komatiite	-0.92	0.07	4
	Komatiite Average (2SE)	-0.872	(0.030)	
	Fresh peridotites			
S-37	spinel lherzolite	-0.91	0.03	4
S-21	spinel lherzolite	-0.90	0.10	4
S-14	spinel lherzolite	-0.93	0.05	4
S-4	spinel lherzolite	-0.85	0.04	4
S-15	spinel lherzolite	-0.91	0.07	4
S-17	spinel lherzolite	-0.90	0.09	4
S-2	spinel lherzolite	-0.93	0.04	4
S-1	spinel lherzolite	-0.95	0.04	4
S-22	spinel lherzolite	-0.92	0.03	4
S-16	spinel lherzolite	-0.92	0.05	4
H-25	Spinel Harzburgite	-0.93	0.03	4
313-1	garnet lherzolite	-0.72	0.15	3
313-6	garnet lherzolite	-0.62	0.15	3
313-102	garnet lherzolite	-0.58	0.07	3
313-104	garnet lherzolite	-0.83	0.22	3
313-106	garnet lherzolite	-0.75	0.03	3
313-112	garnet lherzolite	-0.70	0.15	3
BD 730	garnet lherzolite	-0.99	0.20	3
BD 822	spinel lherzolite	-0.78	0.15	3
314-56	spinel lherzolite	-0.77	0.15	3
314-58	spinel lherzolite	-0.81	0.29	3
Mo 101	spinel lherzolite	-0.64	0.09	3
	Peridotite Average (2SE)	-0.829	(0.050)	

[#] - error bars as reported in each manuscript. The long-term external errors often exceed what was reported for individual samples in these papers and it might be more appropriate to apply these. However, we have not weighted the samples used in the BSE estimate according to individual sample errors and the errors shown here are only for informational purposes.

Table S-2 Vanadium isotope compositions and GCR corrections for chondrites.

Sample	type	V* (µg/g)	Fe# (µg/g)	CRE age§ (Ma)	$\delta^{51}V_{meas}$¶	n	error (2sd)	$\delta^{51}V_{corr}$
EET92002	CK5	91	228042	33.1	-1.32	6	0.15	-1.14
Karoonda	CK4	91	237076	40.2	-1.32	9	0.07	-1.09
ALH83100	CM2	72	216146	0.17	-1.07	2	0.18	-1.07
Mighei	CM2	59	212400	2.2	-1.05	7	0.21	-1.03
DOM 08006	CO3.0	80	240717	19	-1.22	9	0.08	-1.10
Lance	CO3.5	76	236606	5	-1.22	9	0.26	-1.19
Warrenton	CO3.7	66	193920	34.2	-1.24	18	0.11	-1.03
St. Marks	EH5	51	320365	1.05	-1.05	4	0.10	-1.03
Indarch	EH4	50	290000	13.3	-1.39	2	0.15	-1.22
WSG95300	H3.3	66	254226	35	-1.39	3	0.07	-1.11
Borkut	L5	95	215000	12.4	-1.12	2	0.10	-1.06
Alfianello	L6	67	221257	28	-1.26	11	0.12	-1.06
Calliham	L6	65	215000	26	-1.32	2	0.10	-1.13
NWA753	R3.9	78	242899	11	-1.13	8	0.15	-1.05
					weighted average			-1.089
					weighted 2SE			0.029

* - All V concentration data are from (Nielsen *et al.*, 2019) except Indarch and Karoonda, which are from this study

- All Fe concentration data are from (Nielsen *et al.*, 2019) except Indarch, Calliham and Borkut that are group averages from (Wasson and Kallemeyn, 1988), Mighei that is from (Mason, 1963) and Karoonda that is from this study

¶ - All V isotope data are from (Nielsen *et al.*, 2019) except Indarch and Karoonda and four additional analyses of Alfianello, which are from this study

§ - CRE ages from (Mazor *et al.*, 1970; Sarafin *et al.*, 1984; Alexeev, 1998; Wieler *et al.*, 1999; Scherer and Schultz, 2000; Patzer and Schultz, 2001; Schultz *et al.*, 2005; Davidson *et al.*, 2019; Hopkins *et al.*, 2019)

Supplementary Information References

Alexeev, V.A. (1998) Parent bodies of L and H chondrites: Times of catastrophic events. *Meteoritics & Planetary Science* 33, 145-152.

Davidson, J., Alexander, C.M.O.D., Stroud, R.M., Busemann, H., Nittler, L.R. (2019) Mineralogy and petrology of Dominion Range 08006: A very primitive CO3 carbonaceous chondrite. *Geochimica Et Cosmochimica Acta* 265, 259-278.

Hopkins, S.S., Prytulak, J., Barling, J., Russell, S.S., Coles, B.J., Halliday, A.N. (2019) The vanadium isotopic composition of lunar basalts. *Earth and Planetary Science Letters* 511, 12-24.

Mason, B. (1963) The carbonaceous chondrites. *Space Science Reviews* 1, 621-646.

Mazor, E., Heymann, D., Anders, E. (1970) Noble gases in carbonaceous chondrites. *Geochimica Et Cosmochimica Acta* 34, 781-824.

Nielsen, S.G., Auro, M., Righter, K., Davis, D., Prytulak, J., Wu, F., Owens, J.D. (2019) Nucleosynthetic vanadium isotope heterogeneity of the early solar system recorded in chondritic meteorites. *Earth and Planetary Science Letters* 505, 131-140.

Nielsen, S.G., Owens, J.D., Horner, T.J. (2016) Analysis of high-precision vanadium isotope ratios by medium resolution MC-ICP-MS. *Journal of Analytical Atomic Spectrometry* 31, 531-536.

Nielsen, S.G., Prytulak, J., Halliday, A.N. (2011) Determination of Precise and Accurate 51V / 50V Isotope Ratios by MC-ICP-MS, Part 1: Chemical Separation of Vanadium and Mass Spectrometric Protocols. *Geostandards and Geoanalytical Research* 35, 293-306.

Nyquist, L.E., Bogard, D.D., Shih, C.-Y., Greshake, A., Stöffler, D., Eugster, O. (2001) Ages and Geologic Histories of Martian Meteorites. *Space Science Reviews* 96, 105-164.

Patzer, A., Schultz, L. (2001) Noble gases in enstatite chondrites I: Exposure ages, pairing, and weathering effects. *Meteoritics & Planetary Science* 36, 947-961.

Prytulak, J., Nielsen, S.G., Halliday, A.N. (2011) Determination of Precise and Accurate 51V / 50V Isotope Ratios by Multi-Collector ICP-MS, Part 2: Isotopic Composition of Six Reference Materials plus the Allende Chondrite and Verification Tests. *Geostandards and Geoanalytical Research* 35, 307-318.

Prytulak, J., Nielsen, S.G., Ionov, D.A., Halliday, A.N., Harvey, J., Kelley, K.A., Niu, Y., Peate, D.W., Shimizu, K., Sims, K.W.W. (2013) The Stable Vanadium Isotope Composition of the Mantle and Mafic Lavas. *Earth and Planetary Science Letters* 365, 177-189.

Prytulak, J., Sossi, P.A., Halliday, A.N., Plank, T., Savage, P.S., Woodhead, J.D. (2017) Stable vanadium isotopes as a redox proxy in magmatic systems? *Geochemical Perspectives Letters* 3, 75-84.

Qi, Y.H., Wu, F., Ionov, D.A., Puchtel, I.S., Carlson, R.W., Nicklas, R.W., Yu, H.M., Kang, J.T., Li, C.H., Huang, F. (2019) The vanadium isotopic composition of the BSE: constraints from peridotites and komatiites. *Geochimica Et Cosmochimica Acta* 259, 288-301.

Rizo, H., Walker, R.J., Carlson, R.W., Horan, M.F., Mukhopadhyay, S., Manthos, V., Francis, D., Jackson, M.G. (2016) Preservation of Earth-forming events in the tungsten isotopic composition of modern flood basalts. *Science* 352, 809-812.

Sarafin, R., Bonani, G., Herpers, U., Signer, P., Hofmann, H., Nessi, M., Morenzoni, E., Suter, M., Wieler, R., Wölfli, W. (1984) Spallogenic nuclides in meteorites by conventional and accelerator mass spectrometry. *Nuclear Instruments and Methods in Physics Research Section B: Beam Interactions with Materials and Atoms* 5, 411-414.

Scherer, P., Schultz, L. (2000) Noble gas record, collisional history, and pairing of CV, CO, CK, and other carbonaceous chondrites. *Meteoritics & Planetary Science* 35, 145-153.

Schultz, L., Weber, H.W., Franke, L. (2005) Rumuruti chondrites: Noble gases, exposure ages, pairing, and parent body history. *Meteoritics & Planetary Science* 40, 557-571.

Schuth, S., Horn, I., Bruske, A., Wolff, P.E., Weyer, S. (2017) First vanadium isotope analyses of V-rich minerals by femtosecond laser ablation and solution-nebulization MC-ICP-MS. *Ore Geology Reviews* 81, 1271-1286.

Sossi, P.A., Moynier, F., Chaussidon, M., Villeneuve, J., Kato, C., Gounelle, M. (2017) Early Solar System irradiation quantified by linked vanadium and beryllium isotope variations in meteorites. *Nature Astronomy* 1, 0055.

Sossi, P.A., Prytulak, J., O'Neill, H.S.C. (2018) Experimental calibration of vanadium partitioning and stable isotope fractionation between hydrous granitic melt and magnetite at 800C and 0.5 GPa. *Contributions to Mineralogy and Petrology* 173.

Wasson, J.T., Kallemeyn, G.W. (1988) Compositions of chondrites. *Phil. Trans. R. Soc. Lond. Ser. A* 325, 535-544.

Wieler, R., Baur, H., Busemann, H., Heber, V.S., Leya, I. (1999) Noble Gases in Desert Meteorites: Howardities, Unequilibrated Chondrites, Regolith Breccias and an LL7*Workshop on Extraterrestrial Materials from Cold and Hot Deserts*, Pilanesberg, South Africa.

Wu, F., Owens, J.D., Huang, T., Sarafian, A., Huang, K.-F., Sen, I.S., Horner, T.J., Blusztajn, J., Morton, P., Nielsen, S.G. (2019) Vanadium Isotope Composition of Seawater. *Geochimica Et Cosmochimica Acta* 244, 403-415.

Wu, F., Qi, Y., Perfit, M.R., Gao, Y., Langmuir, C.H., Wanless, V.D., Yu, H., Huang, F. (2018) Vanadium isotope compositions of mid-ocean ridge lavas and altered oceanic crust. *Earth and Planetary Science Letters* 493, 128-139.

Wu, F., Qi, Y.H., Yu, H.M., Tian, S.Y., Hou, Z.H., Huang, F. (2016) Vanadium isotope measurement by MC-ICP-MS. *Chemical Geology* 421, 17-25.

Yoshizaki, T., McDonough, W.F. (2020) The composition of Mars. *Geochimica Et Cosmochimica Acta* 273, 137-162.